CIRP Journal of Manufacturing Science and Technology 41 (2023) 453–464

Contents lists available at ScienceDirect

CIRP Journal of Manufacturing Science and Technology

journal homepage: www.elsevier.com/locate/cirpj

Evaluation of microstructure and thermal history for TiC/Inconel 625 MMC deposition through pre-placed laser cladding method with and without the application of ultrasonic vibration

Shrey Bhatnagar [a], Hari Srinivasarao Magham [a], Suvradip Mullick [a,*], Muvvala Gopinath [b]

[a] School of Mechanical Sciences, Indian Institute of Technology Bhubaneswar, India
[b] Department of Mechanical and Aerospace Engineering, Indian Institute of Technology Hyderabad, India

ARTICLE INFO

Available online 27 January 2023

Keywords:
Metal matrix composite
Laser cladding
Pre-placed
Ultrasonic vibration
Thermal history
TiC
Inconel 625

ABSTRACT

The current work presents the deposition of TiC/ Inconel 625 metal matrix composites (MMC) coating through pre-placed powder bed laser cladding method using a Yb-Fiber laser, under two different conditions, with and without the application of ultrasonic vibration to the work-piece with frequency ranging from 28 to 34 kHz. The disintegration of the TiC particles and its distribution in the matrix was observed under various process parameters (laser power, scan speed and vibration frequency), and the microstructural changes were correlated with the molten pool lifetime obtained from the temperature history of the clad layer, captured using an IR-Pyrometer. The laser cladding without the application of vibration was conducted under constant and variable line energy to study the effect of laser interaction time and laser power on the microstructural evolution under fixed and variable heat flux. Higher molten pool lifetime (due to slow scan speed) at constant laser power resulted in higher disintegration of the MMC particles and formation of dendrites, whereas higher laser power under constant heat flux also resulted the same. Further, the application of ultrasonic vibration, specifically a higher vibration amplitude (at lower vibration frequency) was found to be responsible for more uniform distribution of TiC particles due to breaking of agglomerates, which led to higher hardness.

Introduction

In recent years, researchers have done a lot of work in laser cladding of Ni-based super-alloys due to its high corrosion and wear resistance, as well as good workability, especially at high temperatures [8,20]. In order to further improve the mechanical properties, some reinforced particles are incorporated into the matrix to produce metal matrix composites (MMCs). Titanium Carbide (TiC) is one such favorable material because of its high hardness, high thermal stability and good wettability with Ni-based super alloys. Therefore, it acts as a promising reinforced material for laser based MMC deposition.

Cooper et al. [6] investigated the incorporation of different reinforced particles i.e., Al_2O_3, TiC and SiC to Inconel 625 through additive manufacturing method. Among the three types of reinforcement, TiC was found to provide higher hardness without compromising the density. Jiang et al. [13] fabricated TiC/Inconel 625 composite coatings with nano-sized reinforcement by co-axial laser cladding method. The inclusion of nano-sized reinforcement enhanced the coating performance by improving hardness and strength by 10–12%. Hong et al. [11,12] manufactured ultrafine TiC-Inconel 625 parts reinforced composite. Under variable input energy, they successfully obtained the homogenized and fine dispersion of TiC in the matrix to get a solid dense coating with improved wear resistance and tensile property. Hong et al. [11,12] studied the high-temperature oxidation of TiC/Inconel 625 composite parts prepared using the LMD technique. They have reported that with the increase of TiC content in the matrix, the oxidation resistance of the parts at high temperature was improved. Zheng et al. [22] fabricated TiC/Inconel 625 composite coating using Ni coated TiC powder through LENS technique and found that the coated TiC particles in the MMC improved the strength of the coating and bonding strength with the substrate. Chen et al. [4] studied the effect of laser fluence on TiC/IN625 composites prepared by selective laser melting. They have reported the homogeneous distribution of TiC particles, grain refinement, improvement of wear resistance and hardness along with high densification at higher laser fluence (208 J/mm^3).

* Correspondence to: School of Mechanical Sciences, IIT Bhubaneswar, Khurda, Odisha 752050, India.
E-mail address: suvradip@iitbbs.ac.in (S. Mullick).

https://doi.org/10.1016/j.cirpj.2023.01.009
1755-5817/

The performance of the laser cladding majorly depends upon the process parameters, by controlling the same one can ensure a fully functional coating. Therefore, thermal monitoring of the deposition process is an essential technique for quality control of the clad. Bi et al. [2] used different measuring systems such as a photodiode, pyrometer and CCD camera for closed-loop control of process parameters. Emamian et al. [9] studied the monitoring technique for Direct Metal Deposition (DMD) processed Fe-TiC coating and found that cooling is an important parameter in controlling the decomposition and distribution of TiC in the matrix. Muvvala et al. [15,16] presented similar work to investigate the condition of TiC in the matrix for different scan speeds by studying the change in the slope of the solidification shelf.

Few researchers have also tried to induce ultrasonic vibrations into the laser cladding in order to enhance the mechanical properties through microstructural changes. The ultrasonic vibration creates two non-linear effects, acoustic streaming and cavitation [19]. The acoustic streaming induces the stirring effect in the molten pool which homogenizes the distribution of alloying elements in the matrix. In case of the cavitation effect, the cavitation bubbles start to form and collapse inside the molten pool instantly which generates high pressure and temperature shock waves resulting in breaking the dendrites and refining the grains. The effect of ultrasonic vibration on LENS manufactured AISI 630 stainless steel was investigated by Cong and Ning [5]. The vibration assisted LENS process resulted in higher powder usage efficiency along with improved geometrical and microstructural features such as grain refinement, higher bonding strength and reduction in pores. Zhu et al. [23] studied the effect of ultrasonic vibration on laser cladding of Inconel 718. They have reported the refinement of grains, reduction in porosity as well as improvement in the micro-hardness and wear resistance due to the induction of ultrasonic frequency. Under high-frequency micro-vibrations 340–998 Hz vibration frequency and 10 μm amplitude, Li et al. [14] produced WC reinforce Ni-based coatings on Ti6AL4V alloy. At higher frequencies, the hardening phase W_2C was found to be more pronounced, resulting in higher wear resistance and hardness. Zhang et al. [21] studied the effect of ultrasonic vibration on in-situ TiB_2-TiC reinforced Fe-based composite coatings and reported the uniform distribution of ceramic particles, enhanced properties and higher oxidation resistance of coating at higher ultrasonic vibration power.

The molten pool thermodynamics, such as molten pool temperature, cooling rate, and molten pool lifetime, are reported to get affected by laser process parameters, which ultimately have an impact on microstructure as well as the mechanical and surface properties. As a result, studying the thermal history of molten pool using temperature data obtained from the pyrometer is critical for establishing the best processing conditions. The thermal history monitoring may have more interesting role in case of MMC deposition to determine the complete or partial decomposition of reinforced particles. Further, the reinforced particles are expected to behave differently in the molten pool under the application of ultrasonic vibration, due to the effect of acoustic streaming, resulting in the different solidification self. As a result, monitoring of thermal history and microstructural evolution under the application of ultrasonic vibration is an intriguing research area.

In the current work, TiC/Inconel 625 metal matrix composite deposition has been carried out using pre-placed laser cladding method under two different conditions, without and with the application of ultrasonic vibration to the substrate, using a CW mode Yb-Fiber laser with maximum available power of 240 W. The effect of the process parameters (laser power, scan speed and line energy) along with the acoustic streaming has been investigated on the decomposition or fragmentation of the TiC particles in the matrix under variable vibration frequency, in the range of 28–34 kHz. The microstructural changes under different sets of process parameters, as well as due to the acoustic streaming induced by the ultrasonic vibration has been correlated with the molten pool thermal history, specifically with the molten pool lifetime obtained using an IR-Pyrometer. Further, micro-hardness of the deposited layer has been analysed to study the effect of microstructural changes on the same.

Experimental details

Experimental set-up

Laser cladding of pre-placed MMC deposition was carried out using a CW mode Yb-fiber laser system with 1.06 μm wavelength and maximum workable power of 240 W. The ultrasonic unit used in the current study, comprises of a transducer unit consisting four transducers connected in parallel, and a 600 W ultrasonic generator capable to generate vibration with frequency in the range of 26–35 kHz. The transducer unit can provide vibration in vertical direction, along the expected direction of grain growth with vibration amplitude in the range of 5–15 μm. In the current experimental set-up, the power generated by the ultrasonic generator is constant, and therefore the amplitude of vibration reduces with the increase in vibration frequency. Thus, in the current vibration range the relatively higher amplitude can be obtained with frequency of 28 kHz compared to 33 kHz. The ultrasonic vibration system was integrated with the laser system for providing vibration to the work-piece, as illustrated in Fig. 1.

Calibration of IR pyrometer

The temperature of the molten pool was monitored using an IR-pyrometer (Make: Micro Epsilon, Model: CTLM-2HCF3-C3H) with

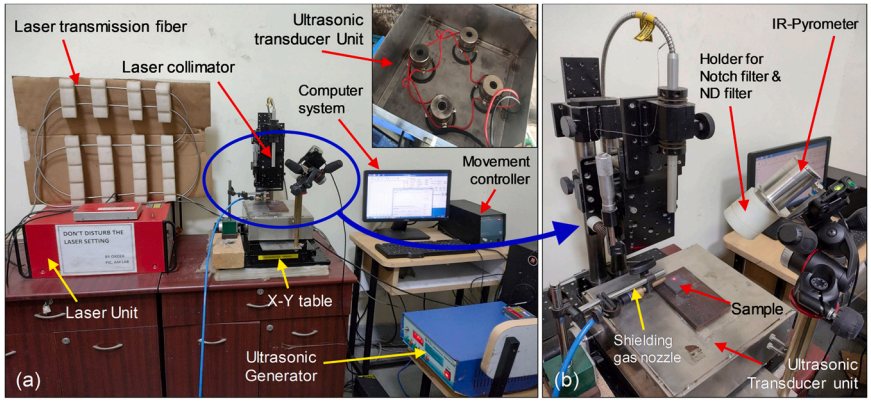

Fig. 1. (a) Experimental set-up for ultrasonic-assisted laser cladding operation and (b) IR-Pyrometer set-up for the online temperature monitoring.

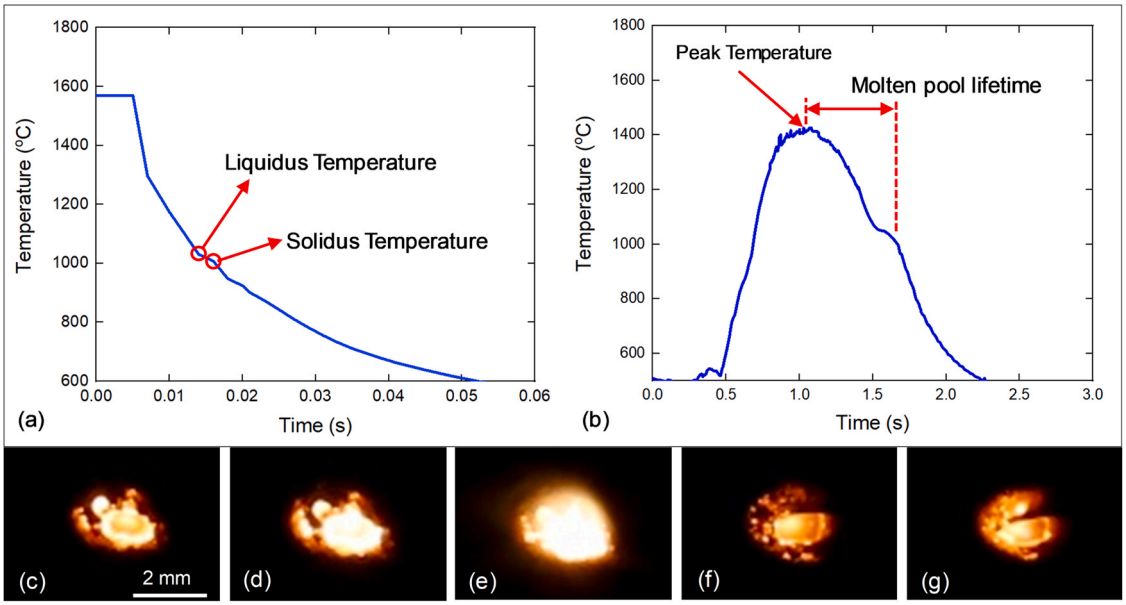

Fig. 2. Thermal images showing (a) solidification shelf observed for melting of AISI 304 Stainless Steel sample, (b) molten pool lifetime observed from the temperature history obtained during the cladding of Inconel; (c)-(g) are the typical high speed photographs of the molten pool taken at an exposure time of 1/4000 s.

spectral wavelength of 1600 nm and working temperature range of 385–1600 °C (non-calibrated temperature range). The pyrometer was fixed on the X-Y movable platform at an angle of about 40° with the vertical and focused at a distance of 200 mm from the substrate to record the signal from the middle of the molten pool. The temperature recorded by the pyrometer was found to detect the reflected or scattered laser radiations. Therefore, a notch filter with a 1064 ± 25 nm spectral range was used to block the scattered laser radiation. Furthermore, a neutral density filter with an optical density of 1.0 was used along with the notch filter to reduce the intensity of the incoming signal to the pyrometer.

The temperature data obtained from the pyrometer readings was calibrated using the temperature reading obtained during laser irradiation of AISI 304 stainless steel plate with known solidus and liquidus temperatures. The pyrometer readings corresponding to the start and end of the solidification slope for SS 304 were obtained from the temperature history, as shown in Fig. 2(a), and the values were compared with the actual solidus and liquidus temperature of the material to find out the calibration factor. Thus, the calibration factor can be expressed as given in Eq. (1), and the average value of the same came around 1.42 with a fluctuation in the range of ± 6%. Further, Fig. 2(b) presents the complete temperature history obtained by the IR pyrometer from a point on the clad track, whereas Fig. 2(c)-(g) are the high speed photographs of the molten pool captured in time sequence using a DSLR camera at an exposure time of 1/4000 s and ISO of 1000 to show the typical nature of the molten pool during the heating and cooling cycle of the deposition process.

$$Calibrationfactor = \frac{Knownsolidus/liquidustemperatureofmaterial}{Respectivepyrometertemperature} \quad (1)$$

Preparation of pre-placed samples

In the current study, metal matrix composite deposition has been carried out using pre-placed laser cladding method with Inconel 625 as matrix and TiC as reinforcement. AISI 304 stainless steel plate of dimensions 30 mm × 30 mm × 8 mm were used as substrate, and substrate surface was polished with abrasive paper (P400 to P600) and cleaned with acetone before coating. IN625 powder (MetcoClad 625, make: Oerlikon Metco) with particle size ranging from 45 to 90 µm and TiC powder with average particle size of 3–15 µm were mixed in a 70:30 wt ratio using a low energy roller milling machine for 8–10 h to achieve uniform distribution. Fig. 3 shows the morphology of the powder particles used as well as the particle size distribution. For TiC powders, it is observed that the maximum percentage of powder particle (more than 75%) are of size less than 5 µm A 5% polyvinyl alcohol aqueous solution was added to the powder mixture to make a thick slurry, and an in-house developed coater was used to apply the slurry to the substrate surface with a homogeneous coating with thickness of 400 µm, where the variation in the thickness of the pre-placed layer developed by the coater was found to be in the range of 2.5–6% of the total layer thickness. The pre-placed powder-coated samples were dried in an oven at 100 °C temperature for around 30 min before the laser irradiation.

Process parameters

The pre-placed samples were irradiated using the focused laser beam having spot size in the range of 900 µm. Argon gas was used as a shielding gas with an operating pressure in the range of 10 bar. The decomposition of ceramic particles in the MMC was found to depend on the heat flux along with the molten pool lifetime, which in turn is a function of laser interaction time to the material, i.e., the laser scan speed. The experiments were carried out under constant and variable line energy by varying the laser power and scan speed, where line energy can be defined as the incident laser energy per unit length of the work-piece, and can be expressed as given in Eq. (2). Further, the experiments were conducted under variable ultrasonic frequency to study the effect of acoustic streaming on the decomposition of the TiC particles. The range of process parameters is illustrated in Table 1.

$$Lineenergy = \frac{Inputlaserpower\,(P_L)}{Scanspeed\,(v)} \quad (2)$$

Sample preparation for Microstructure and material property evaluation

A digital microscope (Model: AM4515ZT, make: Dino-Lite) was used to capture the geometrical features of the deposited layers. The

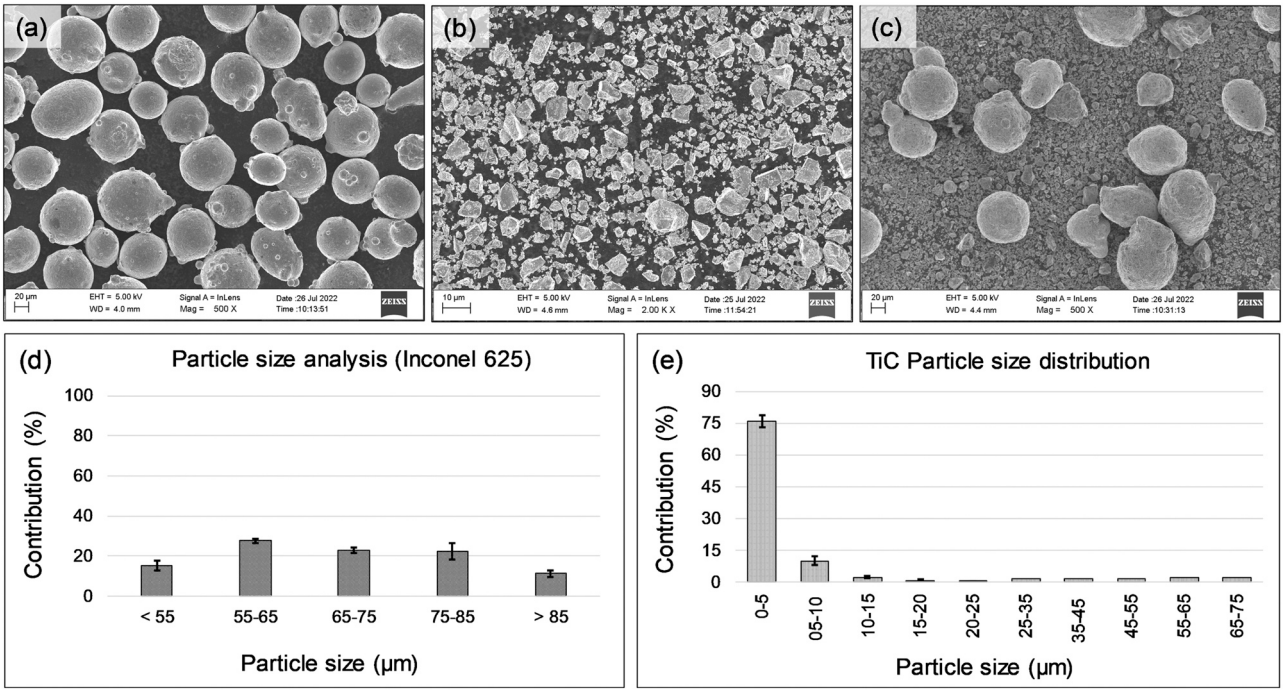

Fig. 3. Morphology of powder particles (a) Inconel 625, (b) Titanium carbide and (c) 30% TiC and 70% IN625; and the particle size distribution of (d) Inconel 625 and (e) TiC particles.

Table 1
Range of input process parameters.

Process Parameter	Experimental Range	Process conditions
Laser power (W)	200, 220 and 240	Variable and Constant line energy
Line energy (J/mm)	93, 109 and 133	
Scan speed (mm/min)	70–180	
Frequency (kHz)	0, 28, 31 and 34	Ultrasonic vibration to the work-piece

microstructure of MMC layer deposited through pre-placed laser cladding was analyzed using a scanning electron microscope (SEM) (Model: ZEISS MERLIN), whereas the elemental study was conducted using energy dispersive spectroscopy (EDX). The hardness values were measured using Vickers micro-hardness tester (Model: ZwickRoell ZHVμ). For the microstructural analysis, the laser cladded MMC samples were cut perpendicular to the laser scan direction using wire-EDM. The cut cross-section of the samples was polished using a series of SiC abrasive papers from P400 to P1500 followed by 1 μm diamond polishing and ultrasonic cleaning for 10 min to get mirrored surface. The clad surface was then etched using a solution of 50 ml HCl, 25 ml HNO_3, and 0.2 gm $CuCl_2{\cdot}2H_2O$ for microstructure appearance. Before microstructure characterization, the etched samples were dried in the oven for 30 min at 100 °C. For micro-hardness analysis, the polished samples before the etching procedure were used. From top to bottom along the clad thickness, several micro-indents of 200 gf and 30 s dwell time were applied. The indents were measured to get hardness values at different locations.

Results and discussion

Influence of process parameters on thermo-cycles

The thermo-cycles obtained using the IR-Pyrometer indicates the maximum temperature along with the rate of heating and cooling during deposition. In the cooling cycle, the molten pool temperature drops suddenly from the peak temperature; after which the slope gradually forms a distinct zone known as a solidification shelf. Formation of this zone is due to the latent heat of fusion of the particular material or alloy, which starts at liquidus temperature and ends at the solidus temperature. The time duration between the peak temperature of the thermo-cycle and solidus temperature of the matrix element is termed molten pool lifetime (shown in Fig. 2(b)), which indicates the time for which the clad volume remains in the molten state (completely or partially). Fig. 4 shows the thermal graphs obtained from the pyrometer under variable and constant line energy conditions. With an increase in scan speed (in the case of variable line energy), the slope of the cooling cycle becomes steeper, resulting in a lower molten pool lifetime.

SEM characterization

SEM analysis under variable line energy (without ultrasonic vibration)

Fig. 5 shows the SEM images of 30% TiC/ Inconel 625 cladded cross-section under variable line energy indicating the microstructural changes due to the change in laser interaction time, whereas Fig. 6 represents the thermal history and molten pool lifetime under those conditions. Higher scan speed at constant laser power leads to lower laser interaction time with the powder layer along with lower heat flux, resulting in shorter molten pool lifetime. The molten pool lifetime is observed to increase with the reduction in the scan speed, as can be seen from the experimental observation, which shows an increase in the molten pool lifetime from 670 ms to 820 ms as the scan speed decreased from 130 to 90 mm/min at constant laser power of 200 W. this also leads to an increase in the line energy from 92 to 133 J/mm. Further, the TiC particles were found to decompose under longer molten pool life time and larger heat flux, forming dendrites. Fig. 5(a) to (c) represent the decomposition of the TiC particles with the reduction in scan speed and increase in molten pool lifetime (as shown in Fig. 6(a) to (c)). Further, the dilution percentage values were calculated using Eq. (3) for the deposited layers under three different line energy conditions. The dilution percentage was observed to increase from 22% to 24% and 28% with the increase in molten pool lifetime. This is due to more interaction time as well as

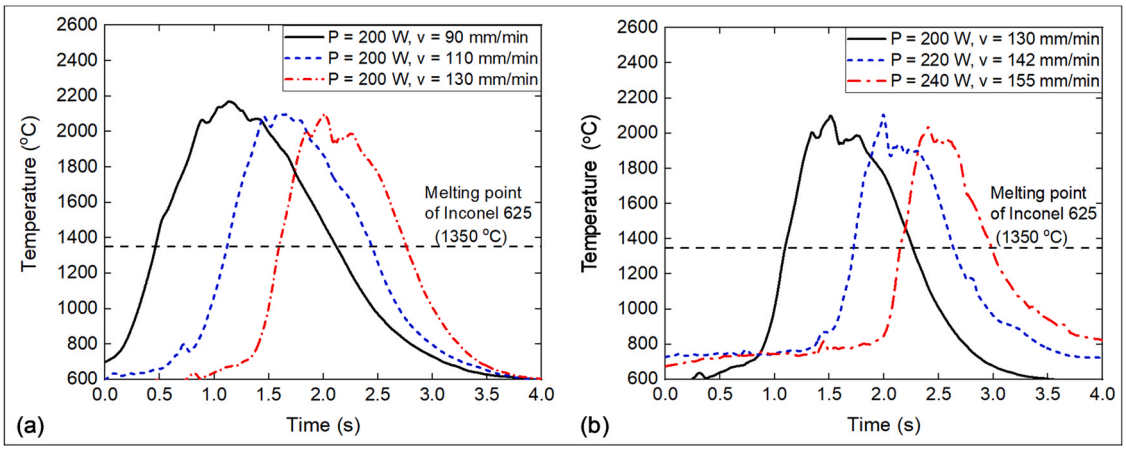

Fig. 4. Thermo-cycles of MMC at various process parameters under (a) Variable line energy at 200 W laser power (b) Constant line energy (93 J/mm).

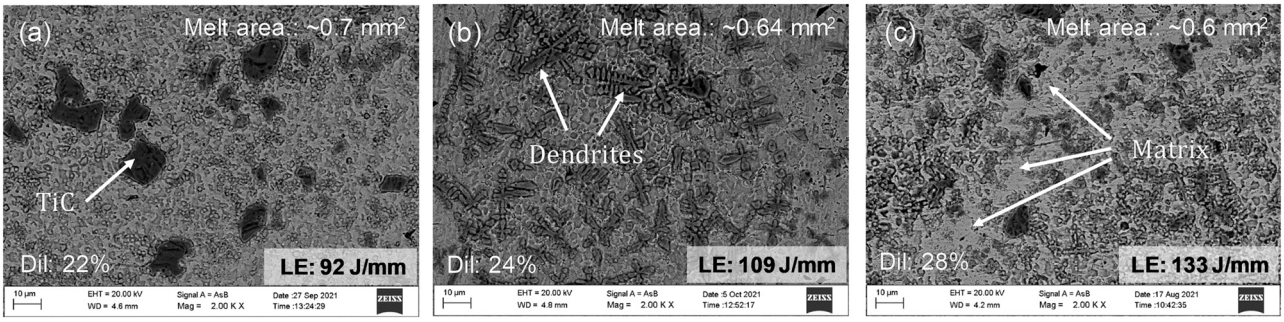

Fig. 5. SEM images showing the behavior of TiC particles in the matrix deposited with different scan speeds of (a) 130 mm/min (b) 110 mm/min and (c) 90 mm/min, under variable line energy with constant laser power of 200 W.

higher laser energy input per unit length (higher line energy) to the work-piece, leading to more heat diffusion to the substrate resulting in higher dilution. Higher dilution at lower speed leads to higher substrate matrix content in the total melt volume, as can be observed in Fig. 5(c). Further, a minor reduction in the melt area is observed with the reduction in scan speed at constant laser power, which may be due to higher conduction loss of the laser energy to the substrate at slower scan speed because of longer interaction time.

$$PercentageDilution = \frac{Cross-sectionalareaofclad}{Cross-sectionalareaof(clad+substratemelting)} \quad (3)$$

Fig. 6(b) shows an extra slope change at a temperature about 1650 °C. This indicates the eutectic reaction, which occurs at the Ti-rich corner at around 1650 °C, according to the Ti and C binary phase diagram [1,18]. As the molten pool gets cooled, the TiC particles starts to nucleate and form dendrites, as shown in the SEM picture captured at a scan speed of 110 mm/min (Fig. 5(b)). The TiC nucleation takes place in the hyper-eutectic range (> 1650 °C) and are followed by a eutectic reaction. As per the Ti-C binary phase diagram the temperature slope varies from the beginning of the hyper-eutectic reaction to the completion of the eutectic reaction. According to the thermal history obtained through IR-pyrometer during the deposition process, this temperature range is 1650–1800 °C. However, the temperature graphs obtained at higher and lower speed of 130 and 90 mm/min, respectively do not show the slope change. Higher speed does not result in formation of dendrites (Fig. 5(a)), whereas at lower speed the significant formation of dendrites is not observed (Fig. 5(c)) due to large matrix content because of higher dilution, which may be the reason for the absence of a distinct slope of eutectic reaction.

Figs. 7–9 shows the elemental mapping of MMC samples under variable line energy conditions, at constant laser power of 200 W. At

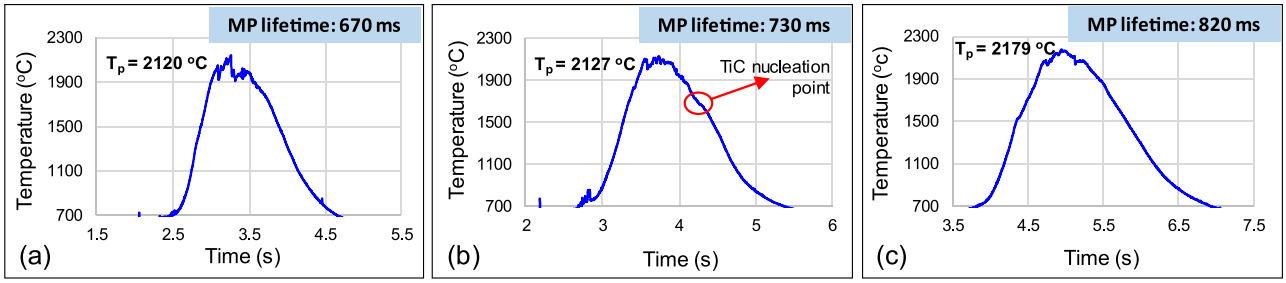

Fig. 6. Temperature history and molten pool lifetime obtained during MMC deposition under laser power of 200 W and scan speed of (a) 130 mm/min (b) 110 mm/min and (c) 90 mm/min.

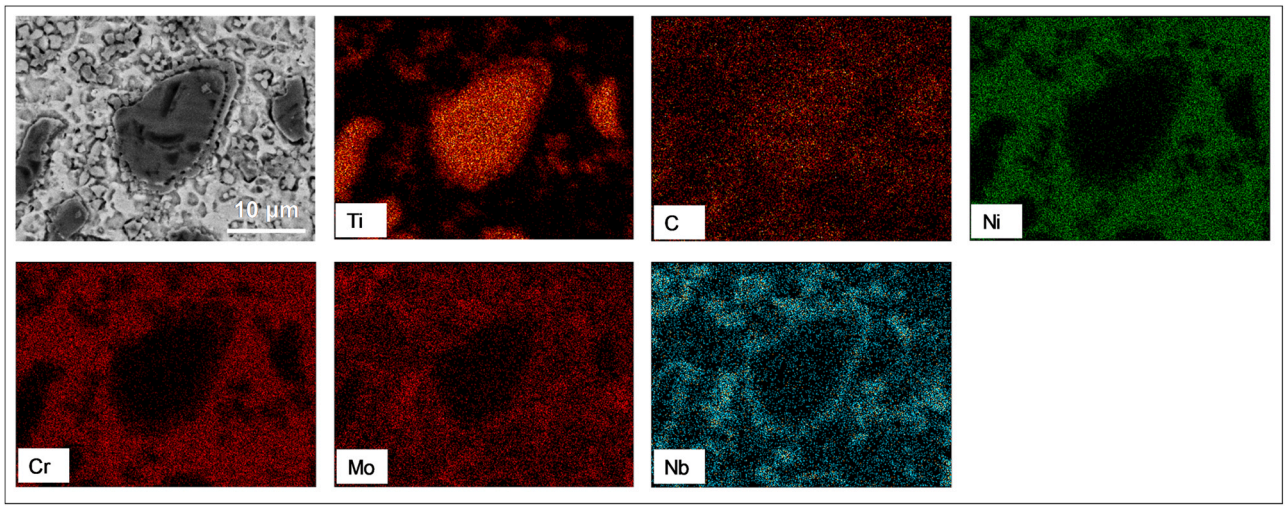

Fig. 7. Elemental mapping of TiC particle at laser power of 200 W and scan speed of 130 mm/min.

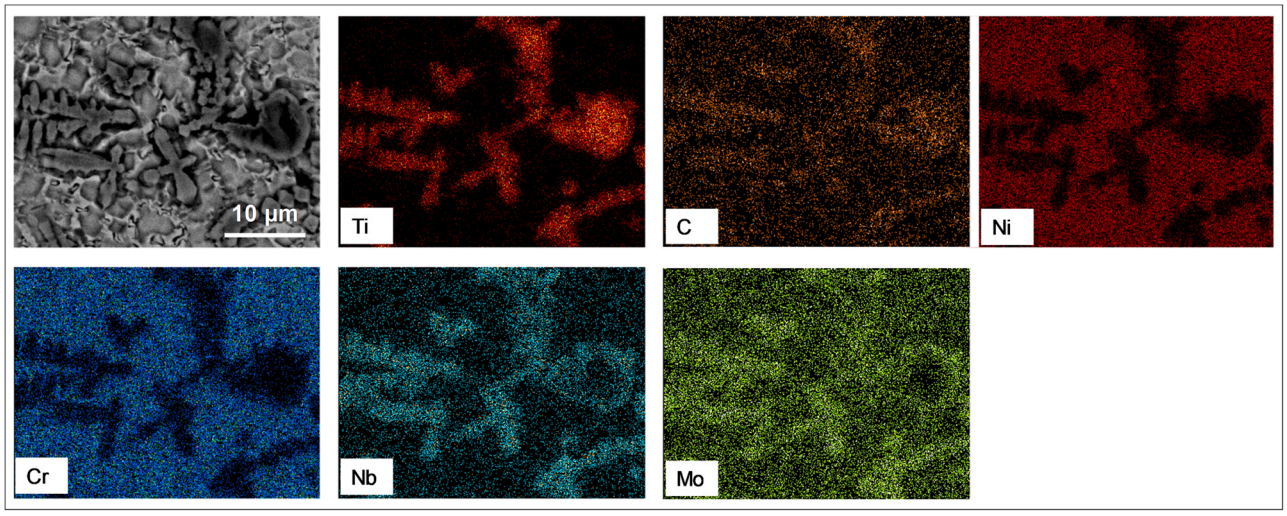

Fig. 8. Elemental mapping of TiC particle at laser power of 200 W and scan speed of 110 mm/min.

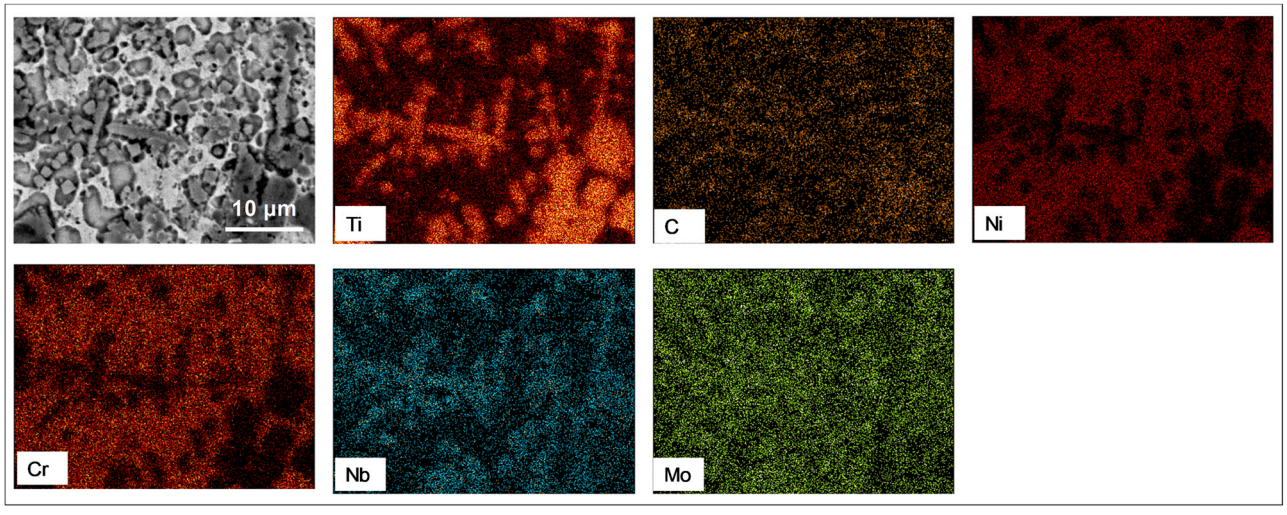

Fig. 9. Elemental mapping of TiC particle at laser power of 200 W and scan speed of 90 mm/min.

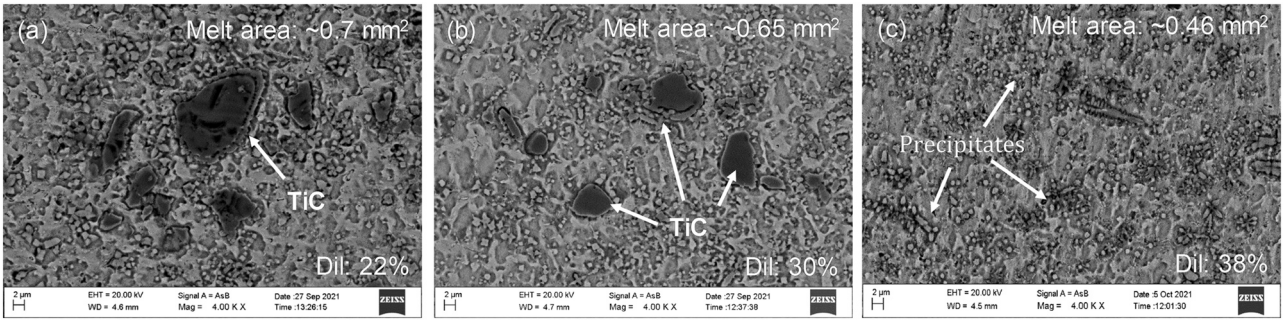

Fig. 10. SEM images showing the behavior of TiC particles in the matrix deposited at different scan speeds under constant line energy 93 J/mm at (a) P = 200 W, v = 130 mm/min (b) P = 220 W, v = 142 mm/min, and (c) P = 240 W, v = 155 mm/min.

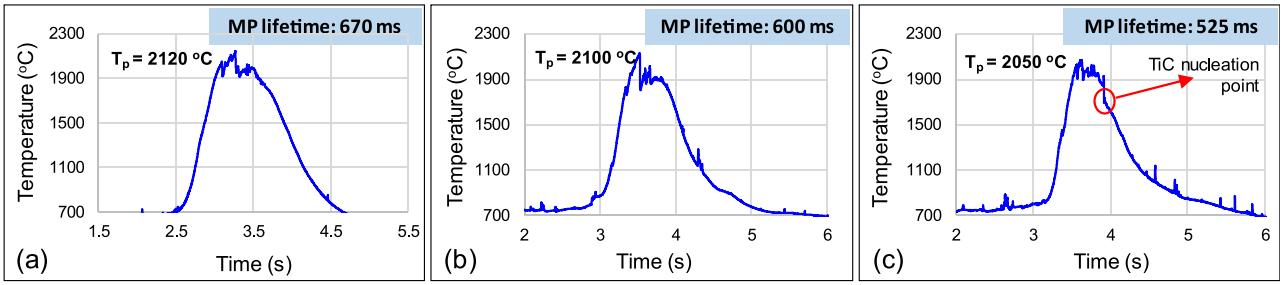

Fig. 11. Temperature history and molten pool lifetime obtained during MMC deposition under (a) P = 200 W, v = 130 mm/min (b) P = 220 W, v = 142 mm/min, and (c) P = 240 W, v = 155 mm/min.

a higher scan speed of 130 mm/min, large TiC particles or agglomerates of TiC were found, surrounded by a reaction layer enriched in Niobium and Molybdenum, forming a shell-core structure (refer Fig. 7). Niobium and Molybdenum segregate around TiC because of their high affinity towards the formation of carbide along with high solubility in TiC [10,15–17]. With the reduction in scan speed, the interaction time increased along with line energy, resulting in larger molten pool lifetime. This promotes the formation of dendrites of carbides rich in Ti, Mo and Nb, as can be seen from the elemental mapping images presented in Figs. 8 and 9.

SEM analysis under constant line energy (without ultrasonic vibration)

The SEM images capturing the microstructural changes due to the simultaneous change in laser power and scan speed under the constant line energy (i.e. constant heat energy per unit length) are shown in Fig. 10, where Fig. 11 represents the thermal history and molten pool lifetime under those conditions. Under a constant line energy condition the effect of laser power was found to have major effect (dominating the effect of molten pool lifetime) on the disintegration of the TiC particles and formation of dendrites.

At lower laser power of 200 W, higher melt volume (larger cross-sectional area, as mentioned in Fig. 10(a)) is observed due to lower scan speed (130 mm/min), resulting in lower temperature (Fig. 11(c)) leading to minimum decomposition of TiC particles (as shown in Fig. 10(a)). An increase in laser power at constant line energy, leads to higher scan speed reducing the melt volume, and thus results in higher molten pool temperature (refer Fig. 11(a)). This causes more disintegration of the TiC particles, resulting in formation of dendrites and precipitates of carbides. The same can be observed in the Fig. 10(b) and (c). However, at laser power of 240 W, excessive

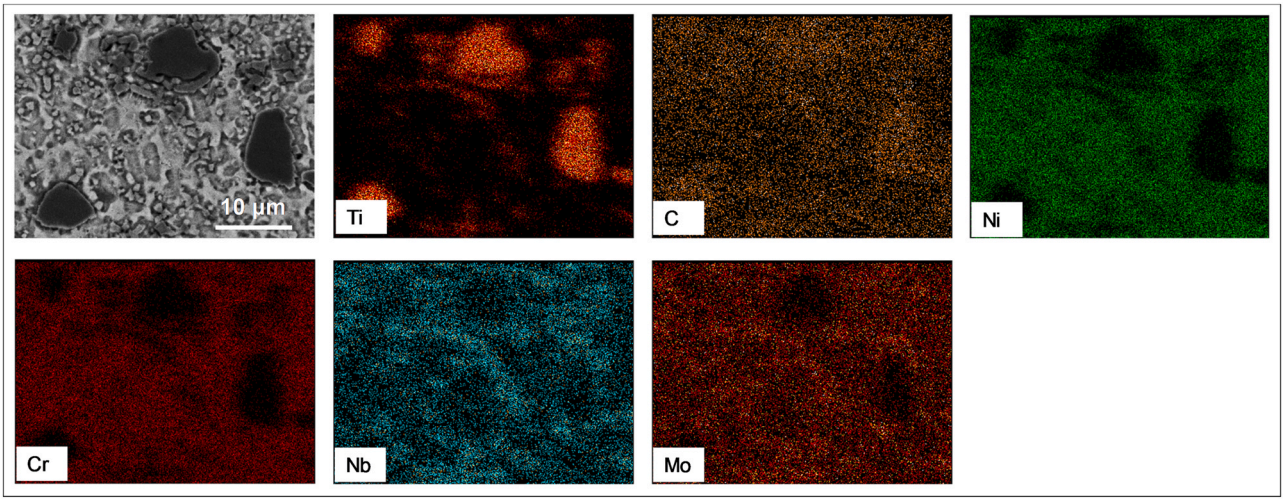

Fig. 12. Elemental mapping of TiC particle at a line energy of 93 J/mm with laser power of 220 W and scan speed of 142 mm/min.

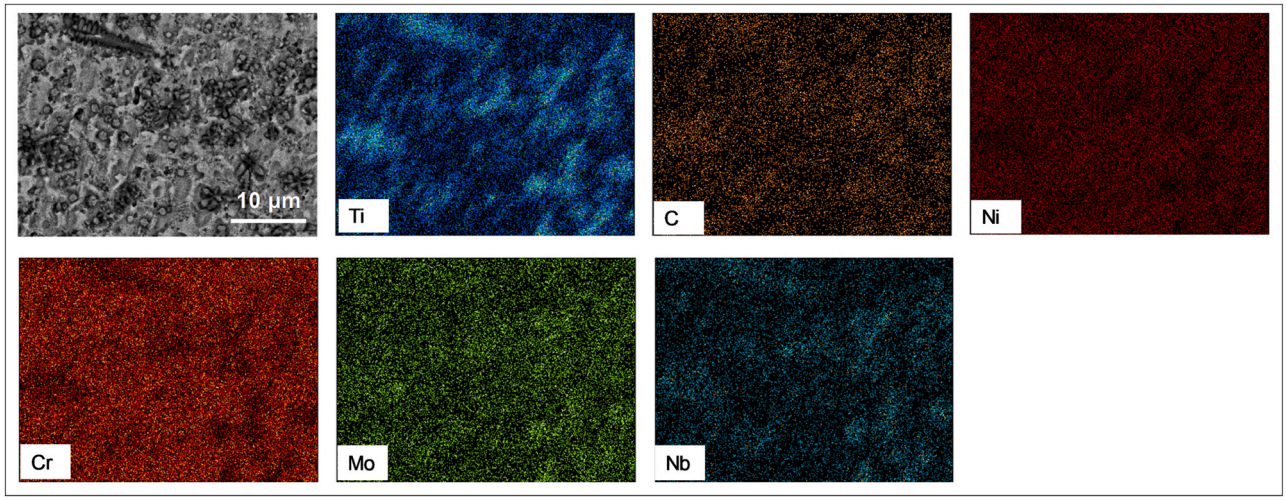

Fig. 13. Elemental mapping of TiC particle at a line energy of 93 J/mm under the laser power of 240 W and scan speed of 155 mm/min.

dilution is observed (around 38%) due to the Gaussian intensity of the laser beam and corresponding high intensity at the center of the beam, resulting in large matrix content.

Similar phenomena of slope change at around 1650 °C is also observed from the temperature history graph obtained for 240 W laser power and 155 mm/min scan speed (Fig. 11 (c)). This is due to the formation dendrites and precipitates of carbides at higher laser power, as observed in the corresponding SEM image (Fig. 10(c)).

The elemental mapping of MMC samples under three different laser power at a constant line energy (93 J/mm) is presented in Figs. 7, 12 and 13. As discussed, deposition under lower laser power results in large size TiC particles and cell-core structure. Whereas, an increase in laser power under constant line energy leads to disintegration of the TiC particles and formation of Nb-rich dendrites and precipitates. However, at highest laser power of 240 W, less amount of dendritic phases is found (refer Fig. 13) due to higher dilution and large matrix content.

Microstructural analysis of the deposition under the application of ultrasonic vibration

Fig. 14 presents the typical microstructural images of TiC/IN625 MMC clad cross-section without and with the application of vibration, which shows the breaking of TiC agglomerates and distribution of fine TiC particles throughout he matrix with the application of vibration. Absence of ultrasonic vibration resulted in agglomerated TiC particles along with non-uniform distribution of the reinforcement particles in the clad, as can be observed from Fig. 14(a), however Fig. 14(b) indicates more uniform distribution of the fine TiC particles throughout the clad section.

Further, Fig. 15 represents the microstructural changes in the deposited layer of MMC under the application of ultrasonic vibration to the work-piece with variable frequency ranging from 28 kHz to 34 kHz, at two different sets of line energy, 80 J/mm and 93 J/mm under constant laser power of 240 W. The amplitude or intensity of vibration is found to reduce with the increase in vibration frequency as the ultrasonic power remains constant. It is found that a lower vibration frequency (under both the set of line energy) resulted in more uniform distribution of the TiC particles in the matrix due to breaking of agglomerates. This is due to higher vibration amplitude at lower frequency, which leads to stronger cavitation effect [23]. Large agglomerates of TiC particles break down and start to disseminate quickly as a result of high-intensity shock waves. At higher frequency, the cavitation intensity is expected to decrease because of lower vibration amplitude, which results in larger TiC particles without significant breaking (as can be seen in Fig. 15 (b) and (e)). The vibration amplitude is minimal at 34 kHz ultrasonic frequency, and therefore does not show any significant effect on TiC distribution (refer Fig. 15 (c) and (f)), instead it shows the presence of agglomerated TiC particles.

The same can be also observed under the condition without ultrasonic vibration (Fig. 15 (d) and (h)). However, the temperature history shows a reduction in molten pool lifetime at lower vibration frequency. Lower vibration frequency leads to higher vibration amplitude resulting in higher intensity of cavitation in the molten pool.

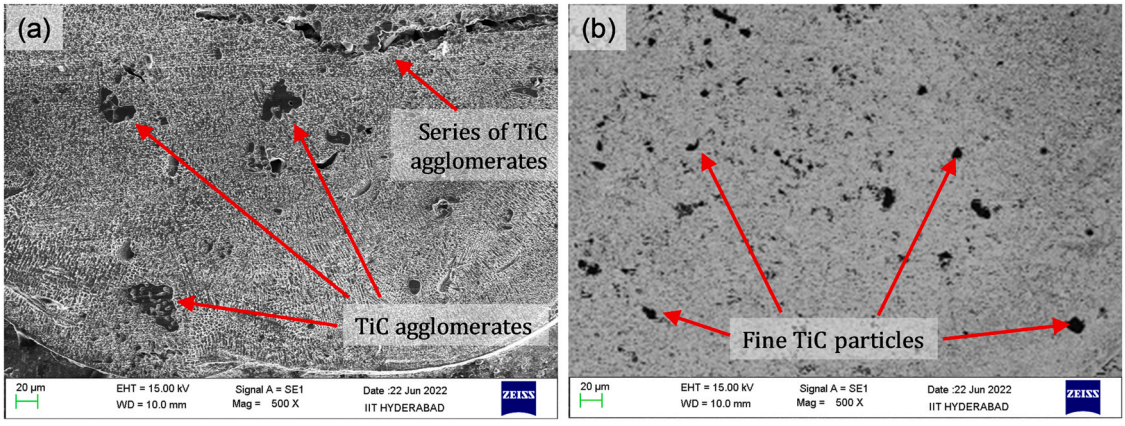

Fig. 14. Typical SEM images of the MMC clad cross-section, (a) without the application vibration and (b) under the application of vibration at 28 kHz frequency.

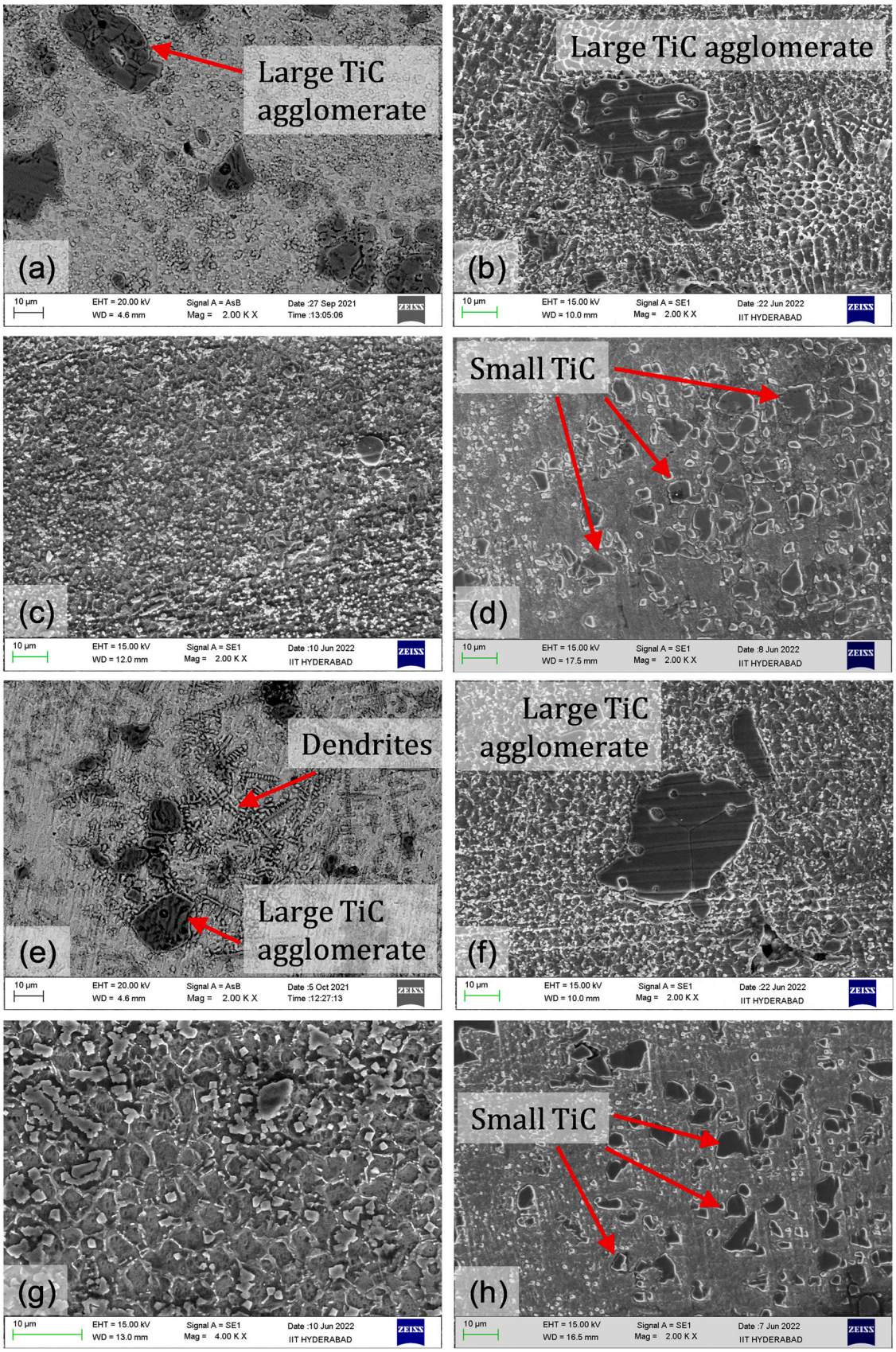

Fig. 15. SEM images showing MMC deposition behavior in the matrix at line energy of (a), (b), (c), (d) 80 J/mm and (e), (f), (g), (h) 93 J/mm under 240 W laser power at an ultrasonic frequency of (a), (e) without vibration (b), (f) 34 kHz, (c), (g) 31 kHz, and (d), (h) 28 kHz.

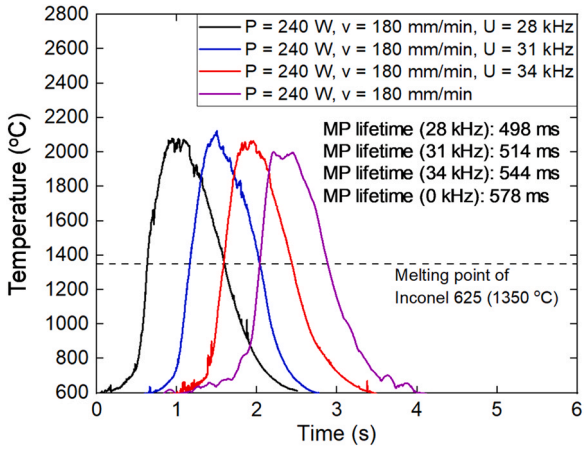

Fig. 16. Temperature history and molten pool lifetime obtained during MMC deposition under the application of ultrasonic vibration at a laser power scan speed of 200 W and 180 mm/min.

This leads to significant breaking of the crystalline grains, resulting in formation of additional nucleation centers reducing the molten pool lifetime [21]. The same can be observed from the thermal history presented in Fig. 16. Therefore, the vibration amplitude has a dominated effect on the molten pool lifetime and discrimination of the reinforcement particles.

Analysis of micro-hardness of deposited layers

The micro-hardness along the depth is measured for the samples deposited with and without the application of ultrasonic vibration. The distance between two indentations along depth is kept in the range of 70 µm, and hardness has been measured along three parallel vertical lines with around 70 µm distance between them. The final hardness value at a particular depth has been estimated by taking the average of those three readings. The hardness values were measured on the cross-section of the deposited MMC layer in such fashion that the indenter would fall on the Inconel matrix and may be partially on TiC particles (but not only on TiC particle or TiC agglomerates), to obtain the overall hardness of the clad layer. Further, the TiC particles are very small in size (maximum numbers of TiC particles are of size less than 5 µm, as can be seen from Fig. 3(e)) and are distributed discretely in the whole clad layer (refer Fig. 14), and therefore the hardness measured specifically on TiC particles (or TiC agglomerates) cannot provide the practical value of hardness of the overall MMC layer.

Micro-hardness of the deposited layer without the application of vibration

The micro-hardness of the cladded samples deposited without the application of ultrasonic vibration is presented in Fig. 17. The Fig. 17(a) presents the change in micro-hardness value due to the change in scan speed under variable line energy, whereas Fig. 17(b) presents the change in micro-hardness value at different laser power under constant line energy. The Fig. 17(a) shows a higher hardness value at higher scan speed under variable line energy. Lower speed results in longer molten pool lifetime and better decomposition of TiC particles (as presented in Fig. 5 and discussed in *SEM analysis under variable line energy (without ultrasonic vibration)*) as well as higher dilution due to longer interaction time. The finer TiC particles get settled in the inter-granular regions of the matrix, increasing the inter-pack spacing [3]. Also, lower speed results in higher dilution, increasing the matrix content. In addition to that, lower scan speed results in larger grain size of the matrix compared to that obtained at higher scan speed [7]. The combined effect results in lower hardness, as can be seen in Fig. 17(a). Similarly, Fig. 17(b) shows a reduction in the hardness value with the increase in laser power at constant line energy. This is because of finer TiC particles due to better decomposition as well as an increase in the matrix fraction due to higher dilution at higher laser power (as presented in Fig. 10 and discussed in *SEM analysis under constant line energy (without ultrasonic vibration)*).

Micro-hardness of the deposited layer under the application of vibration

Fig. 18(a), (b) and (c) presents the change in micro-hardens due to the application of ultrasonic vibration for the MMC layers deposited under three different laser power conditions (200, 220 and 240 W) at a constant line energy of 93 J/mm. The micro-hardness of the cladded samples deposited under the application of ultrasonic vibration is found to have higher value compared to the same obtained during cladding without the application of vibration under different sets of laser power and scan speed. However, at higher frequency of 34 kHz no significant change in the micro-hardness was observed compared to that obtained without vibration at same process parameters.

The above trend can be explained in connection to the microstructural changes shown in Fig. 15. Lower vibration frequency results in higher vibration amplitude, which leads to high intensity acoustic streaming and stronger cavitation effect, which leads to more uniform dissemination of TiC particles in matrix, thus increasing the average hardness. Whereas, lower vibration amplitude at high frequency of 34 kHz could not result in significant breaking and distribution of the TiC particles, which leads to presence of large TiC particles or agglomerates in the matrix, resulting in lower average hardness. A maximum increase in micro-hardness value of

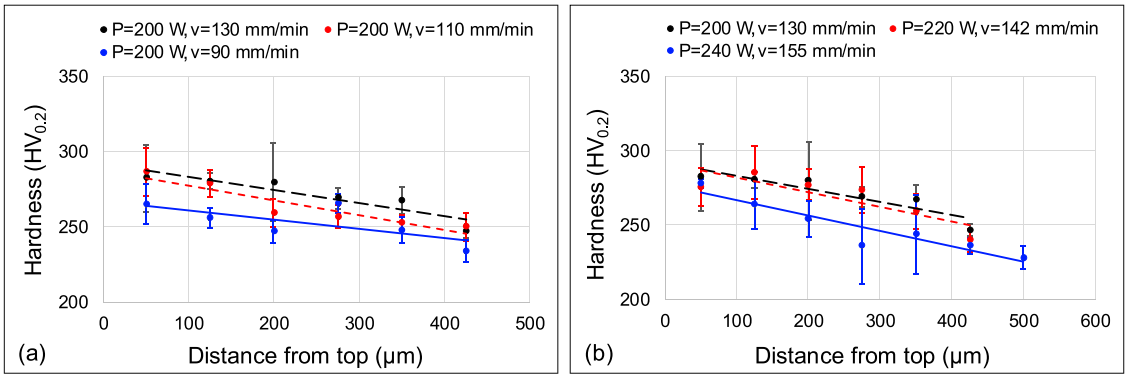

Fig. 17. Micro-hardness distribution from top to bottom layer of the clad at different power and scan speed under (a) variable line energy and (b) constant line energy.

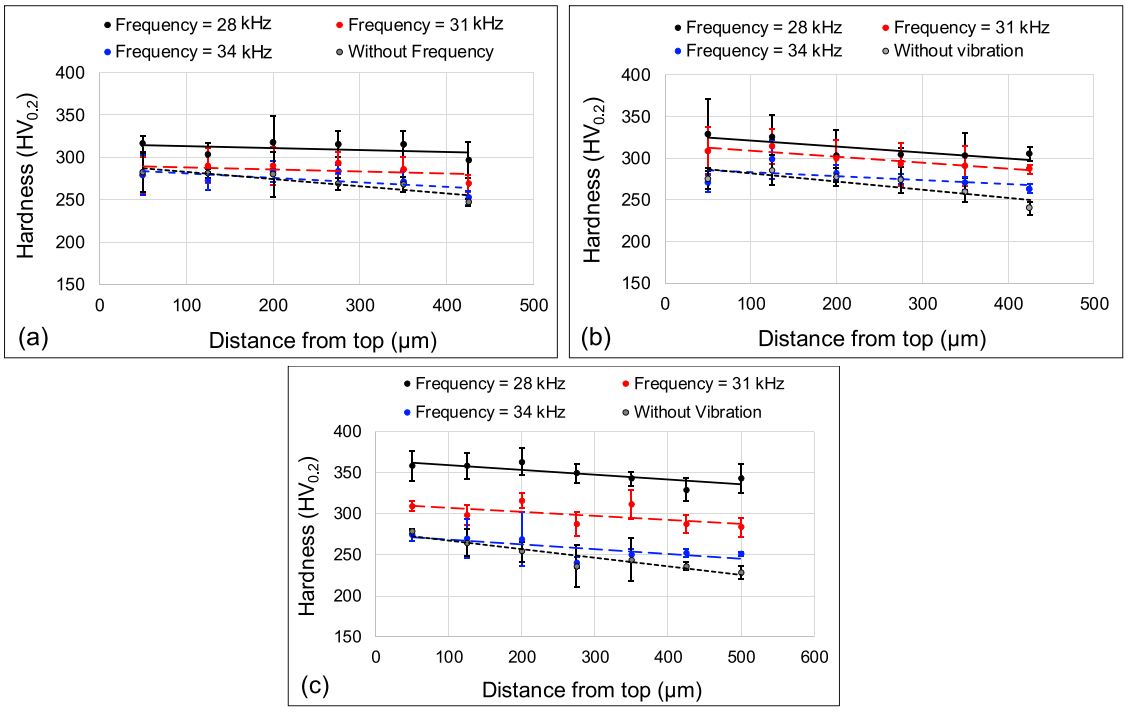

Fig. 18. Micro-hardness distribution from top to bottom layer of the clad at different vibrational frequencies and constant line energy of 93 J/mm at (a) 200 W, (b) 220 W and (c) 240 W input laser power.

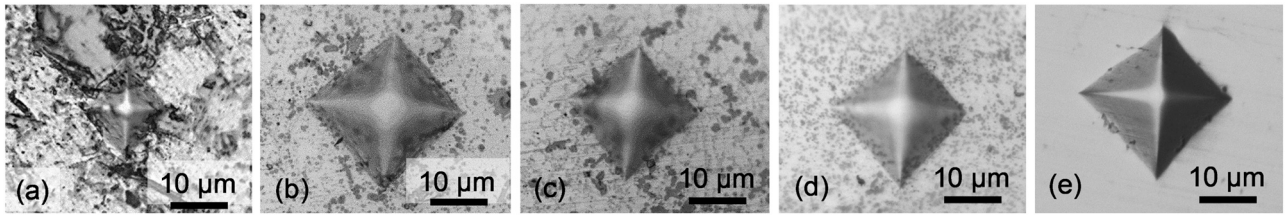

Fig. 19. Typical nature of micro-hardness indentations, on (a) TiC particle, (b) dendrites, (c) sample prepared under 28 kHz frequency, (d) sample prepared under 34 kHz frequency and (e) SS 304 substrate.

33% was observed under 28 kHz vibration frequency compared to no vibration condition.

The typical nature of the indentation profile and size in case of direct indentation on TiC particle, dendrites, indentation on samples deposited at 28 and 34 kHz frequency as well as indentation on AISI 304 SS substrate has been shown in Fig. 19 (a) to (e), respectively. The nature of indentation and its size also indicates the change in micro-hardness value.

Conclusions

TiC/ Inconel 625 metal matrix deposition has been conducted through pre-placed powder bed laser cladding method with 30% TiC content using a Yb-Fiber laser, with and without the application of ultrasonic vibration to the work-piece. The study found the role of molten pool lifetime, laser power as well as vibration amplitude on the decomposition of TiC particles and their distribution in the matrix.

Reduction in scan speed at constant laser power (variable line energy) was found to result in longer molten pool lifetime due to higher laser-material interaction time. This, along with higher heat flux (line energy) at lower speed resulted in higher degree of decomposition of TiC particles in the matrix, as well as the formation of dendrites. However, finer TiC particles resulted in larger inter-pack spacing, leading to lower hardness at lower speed. Further, a very slow speed was found to result in very high dilution, and thus increasing the matrix content.

Increase in laser power at a constant line energy (constant heat flux) resulted in higher degree of decomposition of TiC particles in the matrix, as well as the formation of dendrites due to higher temperature rise. However, higher power at constant line energy results in larger matrix fraction due to higher dilution, which leads to reduction in the hardness value. This also indicated the dominancy of laser power (at constant heat flux) in decomposition of the reinforcement particles even at smaller molten pool lifetime.

The formation of dendrites due to the decomposition of TiC under different set of process parameters can be ensured from the temperature history obtained during the cladding operation, as formation of dendrites slope results in a distinct slope change at around 1650 °C due to the nucleation of TiC particles.

Laser deposition under the application of ultrasonic vibration was found to increase the micro-hardness, specifically at higher vibration amplitude, i.e. at lower vibration frequency of 28 kHz. An increase in micro-hardness value in the range of 15–33% was observed at 28 kHz vibration. Higher vibration amplitude at lower frequency results in high intensity acoustic streaming and stronger cavitation effect, which breaks the large agglomerates of reinforcement particles and also leads to more uniform distribution of the smaller TiC particles throughout the matrix, finally increasing the average hardness.

Declaration of Competing Interest

The authors declare that they have no known competing financial interests or personal relationships that could have appeared to influence the work reported in this paper.

Acknowledgments

Authors gratefully acknowledge the financial support from the Science and Engineering Research Board (under the Department of Science and Technology, Government of India) under the Core Research Grant Program (Grant ID: CRG/2020/002933). The authors gratefully thank Dr. G Bartarya from the School of Mechanical Sciences and Dr. S Gollapudi from the School of Minerals, Metallurgical and Materials Engineering of IIT Bhubaneswar for their support towards conducting the analysis work.

References

[1] Bandyopadhyay, D., Sharma, R.C., Chakraborti, N., 2000, The Ti-Ni-C system (titanium-nickel-carbon). JPE, 21:186.
[2] Bi, G., Gasser, A., Wissenbach, K., Drenker, A., Poprawe, R., 2006, Identification and qualification of temperature signal for monitoring and control in laser cladding. Optics and Lasers in Engineering, 44:1348–1359.
[3] Chen, J., Tang, T., Chan, S., Chang, S., 2008, Effects of particle size on mechanical properties of a TiC containing tool steel by hot isostatic press. Materials Transactions, 49/3: 624–628.
[4] Chen, L., Sun, Y., Li, L., Ren, X., 2020, Microstructure evolution, mechanical properties, and strengthening mechanism of TiC reinforced Inconel 625 nanocomposites fabricated by selective laser melting. Materials Science and Engineering, 792:139655.
[5] Cong, W., Ning, F., 2017, A fundamental investigation on ultrasonic vibration-assisted laser engineered net shaping of stainless steel. International Journal of Machine Tools and Manufacture, 121:61–69.
[6] Cooper, D.E., Blundell, N., Maggs, S., Gibbons, G.J., 2013, Additive layer manufacture of Inconel 625 metal matrix composites, reinforcement material evaluation. Journal of Materials Processing Technology, 213:2191–2200.
[7] Dhanda, M., Haldar, B., Saha, P., 2014, Development and characterization of hard and wear resistant MMC coating on Ti-6Al-4V substrate by laser cladding. Procedia Materials Science, 6:1226–1232.
[8] Dinda, G.P., Dasgupta, A.K., Mazumder, J., 2009, Laser aided direct metal deposition of Inconel 625 superalloy: microstructural evolution and thermal stability. Materials Science and Engineering A, 509:98–104.
[9] Emamian, A., Farshidianfar, M.H., Khajepour, A., 2017, Thermal monitoring of microstructure and carbide morphology in direct metal deposition of Fe-Ti-C metal matrix composites. Journal of Alloys and Compounds, 710:20–28.
[10] Gopinath, M., Mullick, S., Nath, A.K., 2020, Development of process maps based on molten pool thermal history during laser cladding of Inconel 718/TiC metal matrix composite coatings. Surface and Coatings Technology, 399:126100.
[11] Hong, C., Gu, D., Dai, D., Cao, S., Alkhayat, M., Jia, Q., Gasser, A., Weisheit, A., Kelbassa, I., Zhong, M., Poprawe, R., 2015, High-temperature oxidation performance and its mechanism of TiC/Inconel 625 composites prepared by laser metal deposition additive manufacturing. Journal of Laser Applications, 27/S1:S17005.
[12] Hong, C., Gu, D.D., Dai, D.H., Alkhayat, M., Urban, W., Yuan, P., Cao, S.N., Gasser, A., Weisheit, A., Kelbassa, I., Zhong, M., Poprawe, R., 2015, Laser additive manufacturing of ultrafine TiC particle reinforced Inconel 625 based composite parts: tailored microstructures and enhanced performance. Materials Science and Engineering A, 635:118–128.
[13] Jiang, D.F., Hong, C., Zhong, M.L., Alkhayat, M., Weisheit, A., Gasser, A., Zhang, H.J., Kelbassa, I., Poprawe, R., 2014, Fabrication of nano-TiCp reinforced Inconel 625 composite coatings by partial dissolution of micro-TiCp through laser cladding energy input control. Surface and Coatings Technology, 249:125–131.
[14] Li, C., Zhang, Q., Wang, F., Deng, P., Lu, Q., Zhang, Y., Li, S., Ma, P., Li, W., Wang, Y., 2019, Microstructure and wear behaviors of WC-Ni coatings fabricated by laser cladding under high frequency micro-vibration. Applied Surface Science, 485:513–519.
[15] Muvvala, G., Karmakar, D.P., Nath, A.K., 2017, Online monitoring of thermo-cycles and its correlation with microstructure in laser cladding of nickel based super alloy. Optics and Lasers in Engineering, 88:139–152.
[16] Muvvala, G., Karmakar, D.P., Nath, A.K., 2017, Online assessment of TiC decomposition in laser cladding of metal matrix composite coating. Materials and Design, 121:310–320.
[17] Shen, M.Y., Tian, X.J., Liu, D., Tang, H.B., Cheng, X., 2018, Microstructure and fracture behavior of TiC particles reinforced Inconel 625 composites prepared by laser additive manufacturing. Journal of Alloys and Compounds, 734:188–195.
[18] Sun, R.L., Yang, D.Z., Guo, L.X., Dong, S.L., 2001, Laser cladding of Ti-6Al-4V alloy with TiC and TiC+NiCrBSi powders. Surface and Coatings Technology, 135:307–312.
[19] Todaro, C.J., Easton, M.A., Qiu, D., Zhang, D., Bermingham, M.J., Lui, E.W., Brandt, M., StJohn, D.H., Qian, M., 2020, Grain structure control during metal 3D printing by high-intensity ultrasound. Nature Communications, 11:142.
[20] Zahrani, E.M., Alfantazi, A.M., 2014, High temperature corrosion and electrochemical behavior of INCONEL 625 weld overlay in $PbSO_4$–Pb_3O_4–$PbCl_2$–CdO–ZnO molten salt medium. Corrosion Science, 85:60–76.
[21] Zhang, M., Zhao, G.L., Wang, X.H., Liu, S.S., Ying, W.L., 2020, Microstructure evolution and properties of in-situ ceramic particles reinforced Fe-based composite coating produced by ultrasonic vibration assisted laser cladding processing. Surface and Coatings Technology, 403:126445.
[22] Zheng, B., Topping, T., Smugeresky, J.E., Zhou, Y., Biswas, A., Baker, D., Lavernia, E.J., 2010, The influence of Ni-coated TiC on laser-deposited IN625 metal matrix composites. Metallurgical and Materials Transactions A, 635:568–573.
[23] Zhu, L., Yang, Z., Xin, B., Wang, S., Meng, G., Ning, J., Xue, P., 2021, Microstructure and mechanical properties of parts formed by ultrasonic vibration-assisted laser cladding of Inconel 718. Surface and Coatings Technology, 410:126964.